Letter

Predicted Structures of the Active Sites Responsible for the Improved Reduction of Carbon Dioxide by Gold Nanoparticles

Tao Cheng, Yufeng Huang, Hai Xiao, and William A. Goddard III

J. Phys. Chem. Lett., **Just Accepted Manuscript** • DOI: 10.1021/acs.jpclett.7b01335 • Publication Date (Web): 04 Jul 2017

The Journal of Physical Chemistry Letters is published by the American Chemical Society. 1155 Sixteenth Street N.W., Washington, DC 20036

Predicted Structures of the Active Sites Responsible for the Improved Reduction of Carbon Dioxide by Gold Nanoparticles

*Tao Cheng, Yufeng Huang, Hai Xiao and William A Goddard III**

Materials and Process Simulation Center (MSC) and

Joint Center for Artificial Photosynthesis (JCAP),

California Institute of Technology, Pasadena, California 91125, United States

AUTHOR INFORMATION

Corresponding Author

*E-mail: wag@wag.caltech.edu.

ABSTRACT: Gold (Au) nanoparticles (NPs) are known experimentally to reduce carbon dioxide (CO_2) to carbon monoxide (CO), with far superior performance to Au foils. To obtain guidance in designing improved CO_2 catalysts, we want to understand the nature of the active sites on Au NPs. Here, we employed multiscale atomistic simulations to computationally synthesize and characterize a 10 nm thick Au NP on a carbon nanotube (CNT) support, and then we located active sites from quantum mechanics (QM) calculations on 269 randomly-selected sites. The standard scaling relation is that the formation energy of *COOH (ΔE_{*COOH}) is proportional to the binding energy of *CO ($E^{binding}{}_{*CO}$) so decreasing ΔE_{*COOH} to boost the CO_2 reduction reaction (CO_2RR) causes an increase of $E^{binding}{}_{*CO}$ that retards CO_2RR. We show that the NPs has superior CO_2RR because there are many sites at the twin boundaries that significantly break this scaling relation.

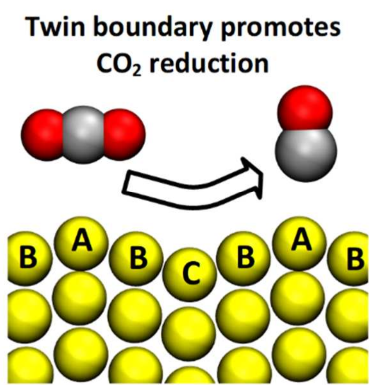

There is great interest in remediating the rapid increase of atmospheric carbon dioxide (CO_2) concentrations with its associated increase in global temperature.[1] One strategy is to develop improved catalysts for the electrochemical reduction of CO_2 to value-added chemicals, such as carbon monoxide (CO), methane (CH_4), ethylene (C_2H_4) and ethanol (C_2H_5OH). [2-3]

Of the metals known to reduce CO_2 to CO efficiently, Gold (Au) exhibits the highest activity and selectivity among polycrystalline metals. As first reported by Hori et al.,[4] the Faradaic efficiency for CO formation is 91% at -1.10 V vs. normal hydrogen electrode (NHE) [or -0.69 V vs. reversible hydrogen electrode (RHE)] with a partial current density of 3.7 mA cm^{-2}. Moreover, Au nanoparticles (NPs) have been shown to improve the CO_2RR performance further. For example, Chen et al. reported that an Au NP derived from Au oxide films results in CO_2RR to CO with Faraday efficiency more than 60% at overpotentials as low as 0.14 V (-0.25Vvs RHE).[5] Feng et al. found a linear relationship between CO_2RR performance and the density of GBs in NPs,[6] concluding that the presence of grain boundaries (GBs) on Au NPs is responsible for the improved CO_2RR performance. In addition, Zhu et al. concluded that for crystalline Au NPs, edge sites are the active sites for CO_2RR.[7-8] They also showed that the size of the Au NPs is critical for controlling reaction rates: 8 nm Au NPs exhibit the best CO_2RR performance,[7] while NPs below 2 nm are active only for hydrogen evolution reactions (HER).[9] Of course, the applied electric field and the electrolyte can also influence CO_2RR. Using Au Nano-needles as catalysts, Liu et al. confirm that a field-induced 20-fold increased surface-adsorbed K^+ ion concentration enables CO_2RR to proceed with a partial current density for CO of 22 mA cm^{-2} at −0.35 V (RHE), the best experimental results reported.[10] Alloying Au[11] or suppressing HER[12] are another directions to improve CO2RR.

Resolving the atomic structure of active sites responsible for the improved performance of Au NPs should provide clues helpful in designing improved CO_2RR catalysts. However, detection of the active sites directly from the experiment has not been possible. We report here computer simulation experiments aimed at synthesizing, characterizing, and resolving the actives sites for CO_2RR on Au NP.

First, we computationally mimic the experimental chemical vapor deposition (CVD) of a 10 nm Au NP on 44.28 nm long, 8.39 nm diameter multiwall carbon nanotube (CNT) support. Here we carried out Reactive Molecular Dynamics (RMD) simulations of Au deposition on a 10nm diameter CNT using the Embedded-Atom Model (EAM) to describe the Au-Au interactions.[13] The CVD experiments use an e-beam evaporated Au source, which we mimic by adding Au atoms into the simulation cell with a deposition rate of 3.0 Å ns^{-1} for 35 ns (the experiment deposition rate is 2 Å s^{-1} for 50 s).

We observed the rapid development of supersaturated Au vapor that in 0.3 ns began to condense. As the concentration of Au vapor reached 0.5 Au atom/nm^3, we observed the formation of Au nuclei containing ~18 atoms on the CNT surface that grew quickly in various directions until their boundaries met. After 35 ns, we obtained a coarse Au NP on CNT with a nominal thickness of about 10 nm, which is consistent with the size of the experimental catalyst.

Then, we employed simulated annealing to heal the defects arising from the fast deposition rate. The peak temperature in the simulated annealing is 1,164K (100K higher than the experimental melting point of Au metal). Each annealing cycle contained a ten ps heating ramp from 300 K to 1,164 K followed by five ps NVT simulation at 1164 K, and then a 10ps cooling ramp from 1,164 K to 300K. Finally, we carried out a 15 ps NVT simulation at 300 K. After 120 such annealing cycles; we found that all grains boundaries disappeared to form a single fullycrystallized Au NP. From the annealing trajectories, we extracted an Au NP structure that most closely resembled the experiment catalyst (after 63 annealing cycles).

To further refine the Au NP structure and the interface between the Au NP and the CNT support, we carried out 20 ps of reactive dynamics at 300 K using the ReaxFF reactive force field trained to reproduce the equation of state of Au FCC metal and the geometry of graphene on the Au (111) surface.[14] Finally, we removed under-coordinated Au atoms (with coordination number less than five) expected to be washed away under the experimental conditions. The final Au NP structure consists of 211,619 atoms (43,200 Carbon atoms + 168,419 Au atoms) with a nominal thickness of 10 nm, as shown in Figure 1A.

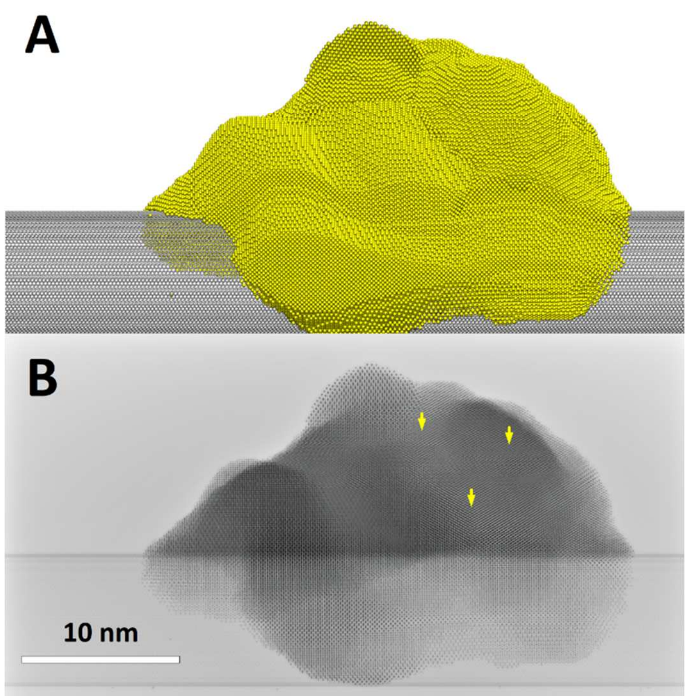

Figure 1. (A) The atomic structure of the Au nanoparticle (NP) "synthesized" computationally by simulating the Chemical Vapor Deposition (CVD) experiment. (B) Predicted Transmission electron microscopy (TEM) images of the predicted Au NP. The yellow marker label three of the grain boundaries (GBs).

This NP leads to an X-Ray Powder Diffraction (XRD) pattern (see Figure S1) showing the typically broadened diffraction peaks of FCC Au due to the small grains, which is consistent with experiment. Our predicted TEM images (Figure 1B) show the GBs in the Au-NP, while our dislocation analysis reveals that 1/6<112> Shockley partial dislocations are the most abundant, leading to stacking faults on the surface. The total length of this dislocation is 3,224 Å, which corresponds to a GB density of 224 μm^{-1} (as defined experimentally).[15] The XRD pattern and TEM images which confirm that the simulated Au NP structure is consistent with experiment.

In our previous work[16] and research from other groups,[17-19] the reaction mechanism of CO_2RR to CO on copper (Cu) is as following:

$$l\text{-}CO_2 \rightarrow *b\text{-}CO_2^{\delta-} \rightarrow *COOH \rightarrow *CO \rightarrow CO \tag{1}$$

In this pathway, physisorbed linear CO_2 [l-CO_2] was first reduced to chemisorbed CO_2 (b-$CO_2^{\delta-}$) facilitated by a partial electron transfer ($\delta \cdot e^-$). In our previous work using PBE-D3 density functional theory (DFT) calculations on the Cu(100) surface with 5 layers of H_2O, we found that b-CO_2^{δ} is in a mixed coordination structure with one C-O bond (1.33 Å) parallel to the surface and one bond (1.29 Å) tilted by ~60°.[16] These distances are close to the C-O bond (1.26) of free CO_2^-.The following proton-coupled electron transfer [$(1\text{-}\delta)\cdot e^-$] reaction leads to *COOH formation, which completes the first electron reduction reaction. The *COOH dehydration reduction reaction leads to *CO formation. Finally, *CO desorbs and releases the reaction site completing the catalysis cycle. In this reaction pathway, b-$CO_2^{\delta-}$ formation is the rate-determining step (RDS), and *COOH formation is the potential-determining step (PDS). Therefore, we took the formation energy of RDS (ΔE_{*COOH}) as a descriptor (as previously proposed by Peterson and Nørskov)[20] to characterize the activity of surface sites toward CO_2RR:

$$\Delta E_{*COOH} = E_{*COOH} - (E_{*} + E_{CO2} + 0.5\times E_{H2}) \tag{2}$$

A lower ΔE_{*COOH} indicates increased CO_2RR. We also calculated the energy of CO desorption (ΔE_{*CO}):

$$\Delta E_{CO} = (E_{*} + E_{CO}) - E_{*CO} \tag{3}$$

This non-electrochemical reaction step determines the rate of CO is leaving the surface sites: the lower ΔE_{*CO} indicates, the higher CO_2RR.

Thus the binding energy of CO can be written as:

$$E^{binding}{}_{*CO} = E_{*CO} - (E_{*} + E_{CO}) = -\Delta E_{*CO} \tag{4}$$

To extract the active sites on Au NP, we randomly selected 269 sites out of 11,360 sites (2.4%) from the catalysis surface. This random sampling introduces no presumptions, ensuring that the statistical distribution represents the overall distribution of the reactive sites. We calculated ΔE_{*COOH} and ΔE_{CO} using cluster models. These cluster models were cut from the simulated nanoparticle by taking the selected sites as the center with a cut-off of 8 Å. Such 8 Å provides a computational accuracy 0.02 eV, which we considered as the best balance of accuracy and efficiency.

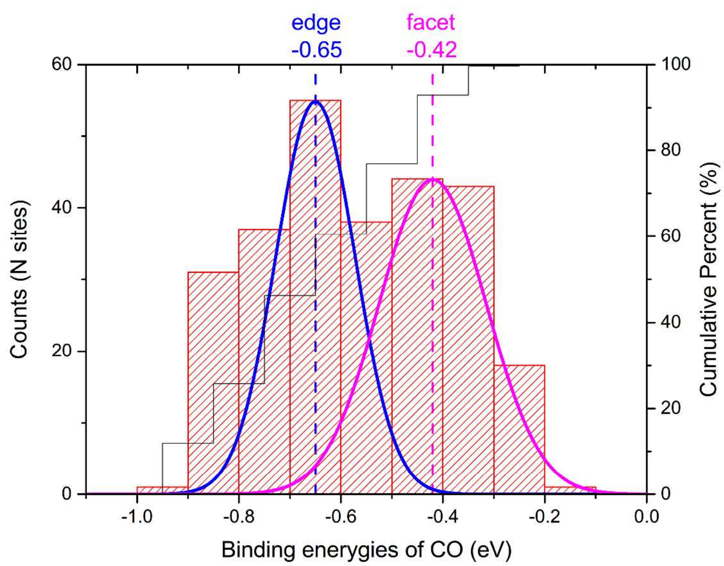

Figure 2. The distribution of CO binding energies ($E^{binding}_{CO}$, in eV) from PBE-D2 DFT on 269 Au NP surface sites selected randomly. The solid black line refers to the right axis as the cumulative percent (%). Two Gaussian functions were employed to fit the binding energies. One takes -0.65 eV (ΔE_{*CO} of edge site) as the center with a width of 0.077 eV (in blue), and the other takes -0.42 eV (ΔE_{*CO} of facet site) as the center with a width of 0.105 eV (in purple).

Figure 2 shows the statistical distribution of $E^{binding}_{CO}$ of 269 surface sites ranging from -0.1 eV to -0.9 eV. To compare with the fully crystalline Au NP, we built an Au octahedron (shown in Figure S2) with a length of 6.93 nm (10,425 Au atoms), which consists of 2,024 facet sites (87.77%), 276 edge sites (11.97%) and six corner sites (0.26%). The DFT CO energy changes (negative is bound), $E^{binding}_{CO}$, are -0.42 eV facet site and -0.65 eV edge site. Taking these two energies as a reference, we fitted the ΔE_{*CO} distribution using Gaussian functions centering at -0.42 eV and -0.65 eV as shown in Figure 2. This fitting indicates that the most abundant binding site are rhombus sites [(111)-like sites] and step sites [(110)-like sites]. These predictions are consistent with experimental electrochemical surface characterizations showing that (111) and (110) facet are dominant.[6] However, the distribution on our CVD derived Au NP is much broader than for the polyhedron crystalline Au NP due to the additional defects created by CVD deposition (primarily GBs and twin boundaries). This broad variation in binding site provides a site library, among which active sites exist responsible for CO_2RR.

We observed the standard scaling relation, a negative correlation between ΔE_{*COOH} and ΔE_{CO} (as shown in Figure 3), with a slope of -0.98. These results are consistent with previous DFT calculations.[21-23] Both small ΔE_{*COOH} (corresponding to a low overpotential) and ΔE_{CO} (promote CO desorption) are favorable to promote CO2RR. The negative correlation indicates that reduction in overpotential (decrease of ΔE_{*COOH}) occurs at the expense of increasing the CO adsorption (an increase of ΔE_{CO}). The sites with strong CO binding (large ΔE_{CO}) are also responsible for promoting the hydrogen evolution reaction (HER), therefore suppressing CO_2RR.[9] The optimal sites for CO_2RR is a balance between ΔE_{*COOH} and ΔE_{CO}. Experimental results suggest that edge sites provide the best balance, increasing activity for CO_2RR. Facet sites have a ΔE_{*COOH} that is too large, leading to high overpotential, while corner sites have exhibited strong binding for *CO and *H, which favors HER. Therefore, the surface sites responsible for promoting CO_2RR on the Au NP are expected to be those highlighted in the upper left part of Figure 3. which exhibit smaller ΔE_{*COOH} without increasing ΔE_{CO} (site α) or reducing ΔE_{CO} without increasing ΔE_{*COOH} (site β) as highlighted in Figure 3.

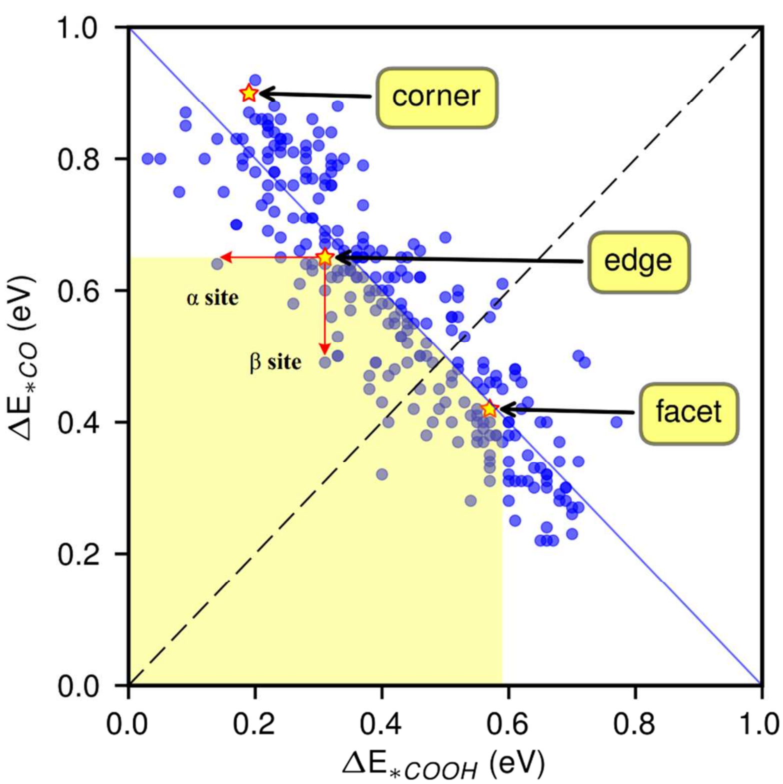

Figure 3. The reaction energy of *COOH formation ((ΔE_{*COOH}) versus the binding energy of *CO (ΔE_{*CO}). The blue circles are the results of 269 surface sites from random sampling. The yellow stars are the results of the facet, edge and corner sites on Au octahedron (as shown in

Figure S2). The yellow filled region highlight the sites breaking linear scaling relationship (promote CO_2RR). The red arrows highlight two sites (α site and β site) with CO_2RR performance better than edge site as predicted.

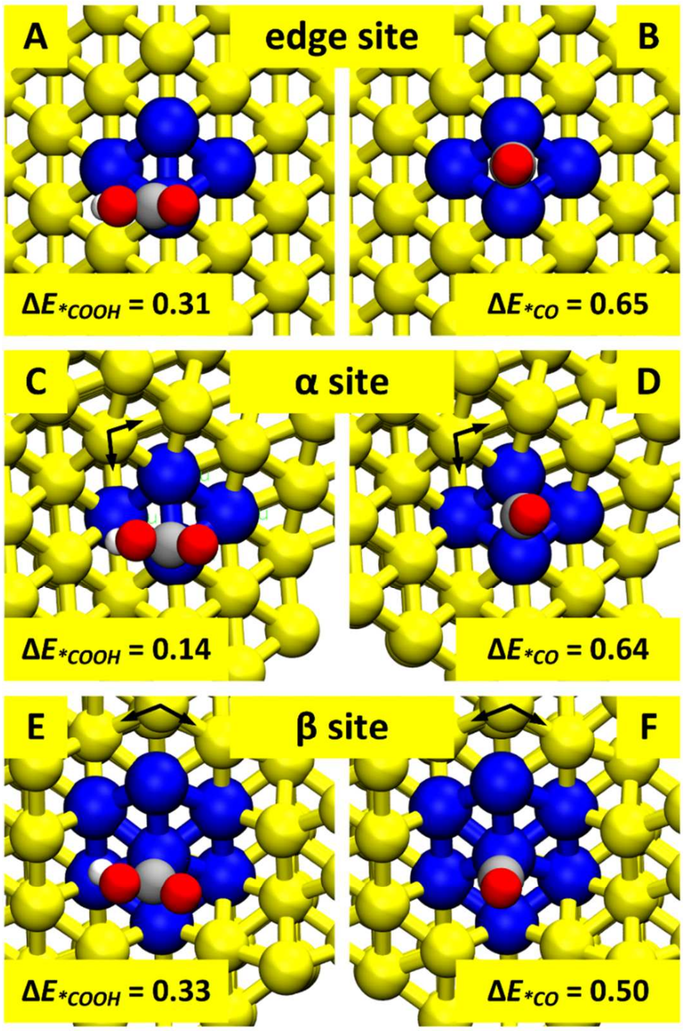

Figure 4. *CO binding on edge site (A), α site (C) and β site (E). *COOH binding on edge site (B), a site (D) and b site (F). The colors are Au in yellow, C in silver, H in white and O in red. We highlighted the binding sites in blue for viewing convenience. Black arrows show the directions of the twin boundaries.

Therefore, these two sites should be superior in increasing CO_2RR. Figure 4C and Figure 4D show *COOH and *CO on α site. Figure 4E and Figure 4F show *COOH and *CO on β site. The common feature of these two sites is that they are on the twin boundaries. To compare, Figure 4A and Figure 4B show *COOH and *CO on edge site. The α site lies on the twin boundary leading to a 0.17 eV decrease in ΔE_{*COOH} (0.14 eV) compared to 0.31 eV for an edge site, while he ΔE_{CO} does not change (0.64 eV vs. 0.65 eV). For the β site, the rhombus site lies on the twin boundary leading to 0.26 eV decrease in ΔE_{*COOH} (0.33 eV) compared with that (0.59 eV) of a facet site, which is very close to the ΔE_{*COOH} (0.31 eV) of an edge site, while ΔE_{CO} decreases by 0.14 eV (0.50 vs. 0.36 eV), which is less than the increase in ΔE_{*COOH}. Therefore, these surface sites on twin boundaries are superior in CO_2RR, because they significantly decrease ΔE_{*COOH}.

To summarize, we employed multiscale simulations to computationally “synthesize” an Au NP with a thickness of 10 nm on a CNT support. The XRD of this Au NP (Figure S1) shows the FCC crystal structure, consistent with the experimental results. The simulated TEM image (Figure 1B) show clear GB structures. A dislocation analysis shows that 1/6<112> Shockley partial dislocations are most abundant, which induces stacking defects on the surface.

To locate the active sites for CO_2RR, we randomly selected 269 response sites out of 11,360 total sites (2.4%) for QM calculations. The QM results show a linear relationship between the ΔE_{*COOH} and ΔE_{CO}, showing that most sites exhibit the normal scaling relationship between *COOH stabilization, *CO desorption, and HER. However, we find a substantial fraction (10%) of NP sites on grain boundaries or twin boundaries that significantly decrease ΔE_{*COOH} without increasing ΔE_{CO}, leading to superior CO_2RR performance.

AUTHOR INFORMATION

Notes

The authors declare no competing financial interests.

ACKNOWLEDGMENT

This work was supported by the Joint Center for Artificial Photosynthesis, a DOE Energy Innovation Hub, supported through the Office of Science of the U.S. Department of Energy under Award No. DE-SC0004993. This work used the Extreme Science and Engineering Discovery Environment (XSEDE) which is supported by National Science Foundation grant number ACI-1053575, and the Zwicky Astrophysics supercomputer at Caltech.

Supporting Information Available: Simulation details, Simulated XRD patterns, Equation of state of FCC Au, an Au octahedral model and ReaxFF parameters of Au and C.

REFERENCES

(1) Foster, G. L.; Royer, D. L.; Lunt, D. J. Future Climate Forcing Potentially Without Precedent in the Last 420 Million Years. *Nat. Commun.* **2017,** *8*, 14845.

(2) Gattrell, M.; Gupta, N.; Co, A. A Review of the Aqueous Electrochemical Reduction of CO_2 to Hydrocarbons at Copper. *J. Electroanal. Chem.* **2006,** *594*, 1-19.

(3) Kortlever, R.; Shen, J.; Schouten, K. J. P.; Calle-Vallejo, F.; Koper, M. T. M. Catalysts and Reaction Pathways for the Electrochemical Reduction of Carbon Dioxide. *J. Phys. Chem. Lett.* **2015,** *6*, 4073-4082.

(4) Hori, Y.; Murata, A.; Kikuchi, K.; Suzuki, S. Electrochemical Reduction of Carbon Dioxides to Carbon Monoxide at a Gold Electrode in Aqueous Potassium Hydrogen Carbonate. *J. Chem. Soc., Chem. Commun.* **1987,** *10*, 728-729.

(5) Chen, Y.; Li, C. W.; Kanan, M. W. Aqueous CO_2 Reduction at Very Low Overpotential on Oxide-Derived Au Nanoparticles. *J. Am. Chem. Soc.* **2012,** *134*, 19969-19972.

(6) Feng, X.; Jiang, K.; Fan, S.; Kanan, M. W. Grain-Boundary-Dependent CO_2 Electroreduction Activity. *J. Am. Chem. Soc.* **2015,** *137*, 4606-4609.

(7) Zhu, W.; Michalsky, R.; Metin, Ö.; Lv, H.; Guo, S.; Wright, C. J.; Sun, X.; Peterson, A. A.; Sun, S. Monodisperse Au Nanoparticles for Selective Electrocatalytic Reduction of CO_2 to CO. *J. Am. Chem. Soc.* **2013,** *135*, 16833-16836.

(8) Zhu, W.; Zhang, Y.-J.; Zhang, H.; Lv, H.; Li, Q.; Michalsky, R.; Peterson, A. A.; Sun, S. Active and Selective Conversion of CO_2 to CO on Ultrathin Au Nanowires. *J. Am. Chem. Soc.* **2014,** *136*, 16132-16135.

(9) Reske, R.; Mistry, H.; Behafarid, F.; Roldan Cuenya, B.; Strasser, P. Particle Size Effects in the Catalytic Electroreduction of CO_2 on Cu Nanoparticles. *J. Am. Chem. Soc.* **2014,** *136*, 6978-6986.

(10) Liu, M.; Pang, Y.; Zhang, B.; De Luna, P.; Voznyy, O.; Xu, J.; Zheng, X.; Dinh, C. T.; Fan, F.; Cao, C., et al. Enhanced Electrocatalytic CO_2 Reduction via Field-Induced Reagent Concentration. *Nature* **2016,** *537*, 382-386.

(11) Lysgaard, S.; Myrdal, J. S. G.; Hansen, H. A.; Vegge, T. A Dft-Based Genetic Algorithm Search for AuCu Nanoalloy Electrocatalysts for CO_2 Reduction. *Phys. Chem. Chem. Phys.* **2015,** *17*, 28270-28276.

(12) Wuttig, A.; Yaguchi, M.; Motobayashi, K.; Osawa, M.; Surendranath, Y. Inhibited Proton Transfer Enhances Au-Catalyzed CO_2-to-Fuels Selectivity. *Proc. Natl. Acad. Sci. U. S. A.* **2016,** *113*, E4585-E4593.

(13) Foiles, S. M.; Baskes, M. I.; Daw, M. S. Embedded-Atom-Method Functions for the FCC Metals Cu, Ag, Au, Ni, Pd, Pt, and Their Alloys. *Phys. Rev. B: Condens. Matter Mater. Phys.* **1986,** *33*, 7983-7991.

(14) Järvi, T. T.; van Duin, A. C. T.; Nordlund, K.; Goddard, W. A. Development of Interatomic Reaxff Potentials for Au–S–C–H Systems. *J. Phys. Chem. A* **2011,** *115*, 10315-10322.

(15) Feng, X.; Jiang, K.; Fan, S.; Kanan, M. W. A Direct Grain-Boundary-Activity Correlation for CO Electroreduction on Cu Nanoparticles. *ACS Cent Sci* **2016,** *2*, 169-174.

(16) Cheng, T.; Xiao, H.; Goddard, W. A. Reaction Mechanisms for the Electrochemical Reduction of CO_2 to CO and Formate on the Cu(100) Surface at 298 K from Quantum Mechanics Free Energy Calculations with Explicit Water. *J. Am. Chem. Soc.* **2016,** *138*, 13802-13805.

(17) Luo, W.; Nie, X.; Janik, M. J.; Asthagiri, A. Facet Dependence of CO_2 Reduction Paths on Cu Electrodes. *ACS Catal.* **2016,** *6*, 219-229.

(18) Nie, X.; Esopi, M. R.; Janik, M. J.; Asthagiri, A. Selectivity of CO_2 Reduction on Copper Electrodes: The Role of the Kinetics of Elementary Steps. *Angew. Chem. Int. Ed.* **2013,** *52*, 2459-2462.

(19) Peterson, A. A.; Abild-Pedersen, F.; Studt, F.; Rossmeisl, J.; Norskov, J. K. How Copper Catalyzes the Electroreduction of Carbon Dioxide into Hydrocarbon Fuels. *Energy Environ. Sci.* **2010,** *3*, 1311-1315.

(20) Peterson, A. A.; Nørskov, J. K. Activity Descriptors for CO_2 Electroreduction to Methane on Transition-Metal Catalysts. *J. Phys. Chem. Lett.* **2012,** *3*, 251-258.

(21) Back, S.; Kim, H.; Jung, Y. Selective Heterogeneous CO_2 Electroreduction to Methanol. *ACS Catal.* **2015,** *5*, 965-971.

(22) Kim, K.-S.; Kim, W. J.; Lim, H.-K.; Lee, E. K.; Kim, H. Tuned Chemical Bonding Ability of Au at Grain Boundaries for Enhanced Electrochemical CO_2 Reduction. *ACS Catal.* **2016,** *6*, 4443-4448.

(23) Back, S.; Yeom, M. S.; Jung, Y. Active Sites of Au and Ag Nanoparticle Catalysts for CO_2 Electroreduction to CO. *ACS Catal.* **2015,** *5*, 5089-5096.